Spontaneous axisymmetry breaking of the external magnetic field at Saturn

Peter Goldreich[1] and Alison J. Farmer[2]

Received 6 November 2006; revised 20 February 2007; accepted 23 February 2007; published 26 May 2007.

[1] Saturn's magnetic field is remarkably axisymmetric. Early evidence for nonaxisymmetry came from the periodicity of Saturn's kilometric radio bursts (SKR). Subsequently, percent-level variations of the SKR period were found to occur on timescales of years. A recent breakthrough has been the direct detection of a nonaxisymmetric component of the field that rotates with a period close to that of the SKR and whose magnitude varies only weakly with distance from Saturn. The latter implies that it must be supported by currents external to the planet. We explore the hypothesis that centrifugally driven convection spontaneously breaks the axisymmetry of the external magnetic field at Saturn. The density of the outflowing plasma close to its source is assumed to contain a substantial part that varies as $\cos\phi$ and rotates uniformly. We demonstrate that the plasma stream must narrow with distance from the planet, while the field-aligned currents joining stream to ionosphere increase rapidly. These currents produce a nonaxisymmetric component of magnetic field whose magnitude varies inversely with radial distance in the planet's equatorial plane. For a rate of plasma outflow $10^4 \lesssim \dot{M} \lesssim 10^5$g s^{-1}, this component's strength is compatible with that observed. Additionally, we postulate that the SKR is associated with the narrow range of longitudes over which large currents flow along magnetic field lines connecting the tip of the outflow to the auroral ionosphere.

Citation: Goldreich, P., and A. J. Farmer (2007), Spontaneous axisymmetry breaking of the external magnetic field at Saturn, *J. Geophys. Res.*, *112*, A05225, doi:10.1029/2006JA012163.

1. Introduction

[2] Saturn's atmosphere exhibits strong (up to 400 m s^{-1}) and stable (over decadal timescales) zonal winds. This precludes assigning a unique rotation period to its outer layers. Although the planet is fluid throughout, its deep interior must be in near solid body rotation (Liu et al., Ohmic dissipation constraint on deep-seated zonal winds on Jupiter and Saturn, submitted to *Icarus*, 2006). The internal rotation would be revealed by observation of nonaxisymmetric components of the planet's magnetic field. This technique works well for Jupiter, but its application to Saturn has been hampered by the extreme axisymmetry of the planet's magnetic field.

[3] Voyager observations of Saturn kilometric radiation (SKR) bursts coming from the planet's auroral regions showed a periodicity of 10 h 39 min 24 ± 7 s [*Desch and Kaiser*, 1981]. The periodicity was suspected to arise from a small nonaxisymmetry of the planet's internally generated magnetic field. Detection of small in situ nonaxisymmetric magnetic components by Voyager and Pioneer 11 magnetometers were also reported [*Giampieri and Dougherty*, 2004], with periods consistent with that of the SKR. Ulysses observations of the variability of the SKR period, by of order 1% on timescales of 1 year from 1994 to 1997 [*Galopeau and Lecacheux*, 2000], challenged its interpretation as the rotation period of the planet's deep interior (a change of 1% in spin period of the planet's core over such a short timescale is energetically impossible). Cassini confirmed this variability, measuring an SKR period of 10 h 45 min 45 ± 45 s on approach to Saturn in 2004 [*Gurnett et al.*, 2005].

[4] Magnetometer data obtained by Cassini revealed a small (few nanotesla) nonaxisymmetric magnetic field component in Saturn's inner magnetosphere whose magnitude declines slowly with increasing distance from the planet [*Giampieri et al.*, 2006]. During 14 months of observation, this component rotated with a period of 10 h 47 min 6 ± 40 s [*Giampieri et al.*, 2006], close to the Cassini SKR period. Henceforth, we assume that the two periods are always equal. *Giampieri et al.* [2006] suggested that this period might be that of Saturn's interior spin. However, the weak radial dependence of the nonaxisymmetric magnetic field components in Saturn's inner magnetosphere implies that they are sourced by local currents.

[5] We propose that the axisymmetry of the external magnetic field at Saturn is spontaneously broken by rotationally driven convection which transports plasma generated in the inner magnetosphere to the magnetopause where it joins the solar wind. It is well known that mass loss by rotationally driven convection must be nonaxisymmetric.

[1] Institute for Advanced Study, Princeton, New Jersey, USA.
[2] Department of Astronomy, Harvard University, Cambridge, Massachusetts, USA.

0148-0227/07/2006JA012163

We assume that a substantial part of the outflow varies as $\cos\phi$. Accepting this assumption, for which supporting evidence [*Gurnett et al.*, 2006] emerged subsequent to the submission of our paper, we show that a mass outflow rate of order a few times 10^4 g s^{-1} can account for both the strength and weak radial dependence of the nonaxisymmetric magnetic field components in Saturn's inner magnetosphere. We emphasize that this form of axisymmetry breaking is independent of nonaxisymmetries of the planet's intrinsic magnetic field. The concept of spontaneous symmetry breaking by rotationally driven convection was in fact developed for and first applied at Jupiter. It is of particular importance at Saturn however, because for Saturn, there does not seem to be any viable alternative, whereas for Jupiter, there is an alternative, as discussed by *Dessler and Hill* [1975, 1979]. Jupiter's intrinsic magnetic field, unlike Saturn's, displays sizable nonaxisymmetric components which rotate at a constant rate. The same period is derived from Jupiter's control of DAM (decametric radiation) and from the rocking of the linear polarization of DIM (decimetric radiation), and it has remained constant to within seconds over 50 years.

[6] The plan of our paper is as follows. In section 2, we provide a simplified version of equations governing rotationally driven magnetospheric convection. We apply these equations in section 3 to estimate the nonaxisymmetric magnetic perturbations it produces. Section 4 is devoted to a discussion of the clock that controls the perturbations' rotation rate. A short summary is given in section 5.

[7] We adopt centimeter-gram-second units for length, mass, time, and Gaussian units for electrodynamical quantities. In order to focus our discussion on Saturn, we provide numerical estimates along with some of the major equations. The parameters used in these evaluations are displayed in Table 1.

Table 1. Adopted Numerical Quantities[a]

Quantity	Value Adopted	Notes
R	6×10^9 cm	
Ω	1.6×10^{-4} s^{-1}	
B_P	0.2 G	
$\Sigma_{\rm p}$	$10^{13}\ \Sigma_{\rm p,13}$ cm s^{-1}	[1]
a_i	$4R\ a_{i,4R}$	[2]
$\Delta\phi_i$	$\pi\ \Delta\phi_i/\pi$	
$\dot{M}$	$10^4\ \dot{M}_4$ g s^{-1}	[3]
μ	3×10^{-24} g	
γ	1.4	
T	$140\ T_{140}$ K	[4]
ν	$10^8\ \nu_8$ cm^2 s^{-1}	[5]
$\rho^{\rm I}$	$3 \times 10^{-13}\ \rho^{\rm I}_{-12.5}$ g cm^{-3}	[6]
g	1×10^3 cm s^{-2}	

[a]The numerical quantities adopted in order of magnitude calculations throughout the paper. The meanings of the symbols are given in the text where first used. Key to numbered notes [1] scaled between estimates for low and high latitude ionosphere [*Atreya et al.*, 1984]; [2] scaled to orbit of E ring; [3] scaled to estimates for plasma production from Saturn's E ring [*Leisner et al.*, 2006]; [4] scaled to atmospheric temperature at base of ionosphere [*Atreya et al.*, 1984]; [5] scaled to eddy diffusion coefficient at homopause [*Atreya et al.*, 1984]; [6] scaled between estimates for low latitude ionosphere and auroral ionosphere [*Atreya et al.*, 1984].

2. Basic Electrodynamics

2.1. Rotationally Driven Magnetospheric Convection

[8] The topic has an extensive history, but this is not the place to review it. Instead, we point to a few influential papers that aided our understanding. We have done nothing more than to apply what we learned from reading the literature.

[9] Equations governing rotationally driven convection were formulated by *Chen* [1977] and by *Hill et al.* [1981]. Many applications have been made to the outward transport of mass from the Io plasma torus. *Pontius and Hill* [1989] included a clear discussion of different approaches to this problem.

[10] Progress in solving the equations referred to above has been slow. In retrospect, this is not surprising. They are a nonlinear set, which probably precludes finding analytic solutions. Moreover, realistic applications are faced with including a continuous supply of plasma along with boundary conditions that simulate its loss to the solar wind at the magnetopause.

[11] The work of *Summers and Siscoe* [1982] is the only paper we have found that considers steady state convection with continuous plasma production. Perhaps the most ambitious attempts at a realistic solution are those of *Yang et al.* [1994] and *Wu et al.* [2007] which apply the Rice convection model to the Io torus. These investigate an initial value problem, the instability of a torus of finite width. An active source of plasma is not included. Thus no account is taken of charge exchange reactions and the ionization of neutrals by electron impact and photoionization.

[12] Convective instability of a torus favors modes whose azimuthal spacing is comparable to the torus' radial width. Indeed, this is what *Yang et al.* [1994] and *Wu et al.* [2007] deduce from their simulations. Long fingers grow radially outward from the torus. This is not surprising. The initial state is analogous to that of a heavier fluid resting on top of a lighter one, which is Rayleigh-Taylor unstable. But unlike the standard Rayleigh-Taylor instability which takes place for constant gravitational acceleration, the instability of the plasma torus is driven by centrifugal acceleration which increases linearly outward. This increase allows narrow fingers to run away from the more slowly developing, thicker modes that might otherwise subsume them.

[13] Plasma generation by the electron impact ionization of neutrals may be by itself a source of nonaxisymmetric instability since the generation rate is proportional to the product of the plasma and neutral densities. Thus perturbations in the plasma surface density could be subject to exponential growth. This is an ingredient that a realistic treatment of rotationally driven convection must include.

[14] In situ observations offer the potential to provide information about the convection pattern in realistic circumstances. However, even after completion of the Galileo mission, not much is known about the pattern of rotationally driven convection in Jupiter's magnetosphere [*Krupp et al.*, 2004].

2.2. A Simplified Model

[15] We explore the hypothesis that centrifugally driven convection spontaneously breaks the axisymmetry of the external magnetic field at Saturn. In order to account for the data, we assume that the outflowing plasma has a substantial component whose surface density varies as $\cos\phi$ with azimuth. This component will be referred to as the plasma

tongue. Except within the tongue, flux tubes outside the torus drift inward because of "fringing" electric fields surrounding the tongue region. As they cross the torus, the inward-moving tubes are loaded with freshly created plasma. Then their trajectories bend around so that they join the back of the tongue. In this manner, plasma is continuously removed from the entire torus even though the tongue emanates from only a limited range of azimuth.

[16] In order for the convection pattern to remain steady, plasma must consistently flow out from the same range of azimuth in the rotating frame. Outflow occurs from the densest part of the torus, and so if a single tongue is to carry the outgoing material, its base must always be refilled fast enough so that no other longitude in the torus can accumulate more plasma. Only if the base of the tongue spans $\Delta\phi_i \lesssim \pi$ radians can the inward drift velocity be large enough to keep the plasma content in the rest of the torus lower than in the tongue region.

[17] We have been able to bolster this description with simplified models of electrostatic fields, but much remains to be done before anything rigorous might emerge. A serious technical issue is that a smooth tongue of plasma is likely to develop narrower fingers as discussed above. Fortunately, the conclusions of our investigation are insensitive to this possibility. However, it would certainly impede a rigorous calculation of the convection pattern. That will have to be left for the future.

2.3. Enceladus as the Source

[18] HST observations of a torus of OH molecules orbiting Saturn indicated a source of $\sim 10^5$g s^{-1} of H_2O molecules near Enceladus [*Shemansky et al.*, 1993; *Jurac et al.*, 2002]. That the satellite itself is the source was revealed by Cassini during a close encounter [*Hansen et al.*, 2006; *Tokar et al.*, 2006; *Pontius and Hill*, 2006]. Close to Enceladus, the lifetime of a neutral molecule to charge exchange is of order months, with ionization by electron impact being an order of magnitude slower [*Johnson et al.*, 2006; *Tokar et al.*, 2006]. This implies a lower limit of $\sim 10^4$g s^{-1} for the plasma creation rate because some of the hot neutrals produced from charge exchange remain bound; *Johnson et al.* [2006] estimates this fraction to be ≈ 0.3.

2.4. Notation

[19] We adopt spherical polar coordinates r, θ, ϕ, and work in the inertial frame. Saturn's magnetic field is approximated as a spin-aligned dipole. The ionosphere is taken to rotate with uniform angular velocity Ω (except in section 4 where Ω denotes the angular velocity of the deep atmosphere). Where necessary, superscripts M and I are used to distinguish magnetospheric and ionospheric quantities, and superscripts Ip and Ih are used to denote the Pedersen (direct) and Hall components of the ionospheric current. B_r and B_θ are the components of the unperturbed magnetic field at a general field point. R is Saturn's radius, and a is the orbital radius in the equatorial plane. B_P is the magnetic field intensity on the equator in Saturn's ionosphere, and B_z is the component of the vertical magnetic field in the magnetic equator at a;

$$B_z = -\left(\frac{R}{a}\right)^3 B_P. \tag{1}$$

Height-integrated current densities and electrical conductivities are indicated by J and Σ, respectively. The surface mass density in the magnetosphere is denoted by σ.

2.5. Dipole Magnetic Fields

[20] Components of a spin aligned dipole magnetic field take the form

$$B_r = \frac{2M\cos\theta}{r^3} \qquad B_\theta = \frac{M\sin\theta}{r^3}\,, \tag{2}$$

where M is the dipole moment. The field magnitude is

$$B = \left(B_r^2 + B_\theta^2\right)^{1/2} = \frac{M}{r^3}\left(1 + 3\cos^2\theta\right)^{1/2}. \tag{3}$$

[21] An individual field line is labeled by either the colatitude of its footprint at $r = R$, denoted by θ_0 or by its maximum radial extent a; $a\sin^2\theta_0 = R$. Its shape is described by:

$$r\sin^2\theta_0 = R\sin^2\theta \qquad \text{or} \qquad r = a\sin^2\theta\,. \tag{4}$$

[22] We are interested in field lines that connect to the planet at high latitudes. Thus we simplify our expressions by setting $\sin\theta_0 = (R\,/\,a)^{1/2}$ and $\cos\theta_0 = 1$.

2.6. Magnetospheric Currents

[23] Consider an element of cold plasma that is nearly corotating with and slowly drifting away from the planet. Centrifugal balance and angular momentum conservation require that the height-integrated current densities which pass through the element satisfy

$$\frac{J_\phi^{\mathrm{M}} B_z}{c} = -\sigma\Omega^2 a \tag{5}$$

and

$$\frac{J_a^{\mathrm{M}} B_z}{c} = -2\sigma\Omega\dot{a} \tag{6}$$

respectively, where we have neglected the planet's gravity in equation (5).

[24] The ratio

$$\frac{J_a^{\mathrm{M}}}{J_\phi^{\mathrm{M}}} = \frac{2\dot{a}}{\Omega a} \tag{7}$$

is small in the inner magnetosphere but becomes of order unity in its outer regions.

[25] The horizontal divergence of the magnetospheric currents, $\nabla_{2d}\cdot\mathbf{J}^{\mathrm{M}}$, flows along magnetic field lines and into the ionosphere. It is the source for the electric field in the ionosphere.

2.7. Ionospheric Electric Field

[26] The height-integrated current density, $\mathbf{J}^{\mathrm{I}}$, and electric field, $\mathbf{E}^{\mathrm{I}}$, are related by

$$\mathbf{J}^{\mathrm{I}} = \mathbf{J}^{\mathrm{Ip}} + \mathbf{J}^{\mathrm{Ih}} = \Sigma_p\mathbf{F}^{\mathrm{I}} + \Sigma_h\left(\hat{\mathbf{b}}\times\mathbf{E}^{\mathrm{I}}\right), \tag{8}$$

where $\mathbf{F}^{\rm I} \equiv \mathbf{E}^{\rm I} + (\mathbf{\Omega} \times \mathbf{R}) \times \mathbf{B}^{\rm I}/c$ is the Lorentz force, $\Sigma_{\rm p}$ and $\Sigma_{\rm h}$ are the height-integrated Pedersen and Hall conductivities, and $\mathbf{b} \equiv \mathbf{B}^{\rm I}/|\mathbf{B}^{\rm I}|$. By setting $\sin\theta_0 = (R/a)^{1/2}$ and $\cos\theta_0 = 1$, we neglect both $B^{\rm I}_\theta$ and the effects of the parallel conductivity. Taking the divergence of equation (8) yields

$$\nabla_{2d} \cdot \mathbf{J}^{\rm I} = \nabla_{2d} \cdot \mathbf{J}^{\rm Ip} = \Sigma_{\rm p} \nabla_{2d} \cdot \mathbf{E}^{\rm I} . \tag{9}$$

We assume that the Hall conductivity is independent of position so $\nabla_{2d} \cdot \mathbf{J}^{\rm Ih} = 0$ because $\nabla_{2d} \times \mathbf{E}^{\rm I} = 0$; $\mathbf{E}^{\rm I}$ is a potential field. A full solution for $\mathbf{E}^{\rm I}$ would involve setting $\mathbf{E} = -\nabla\Phi^{\rm I}$ and then solving Poisson's equation $\nabla^2\Phi^{\rm I} = -\Sigma_{\rm p}\nabla_{2d} \cdot \mathbf{J}^{\rm Ip}$. As detailed in section 2.1, for realistic conditions, this has proven to be a difficult task. Fortunately, an approximate procedure suffices for the current investigation.

[27] We simply map $\mathbf{J}^{\rm M}$ to $\mathbf{J}^{\rm Ip}$. Specifically, we set

$$J^{\rm Ip}_\phi = \frac{1}{R}\frac{{\rm d}a}{{\rm d}\theta_0}\frac{J^{\rm M}_\phi}{2} = -\frac{c\sigma\Omega^2 R}{B_P}\left(\frac{a}{R}\right)^{11/2} , \tag{10}$$

and

$$J^{\rm Ip}_\theta = \frac{a}{R\sin\theta_0}\frac{J^{\rm M}_a}{2} = \frac{c\sigma\Omega R}{B_P}\left(\frac{a}{R}\right)^{11/2}\frac{\dot a}{a} . \tag{11}$$

[28] Their ratio is given by

$$\frac{J^{\rm Ip}_\theta}{J^{\rm Ip}_\phi} = -\frac{\dot a}{\Omega a} . \tag{12}$$

Determination of $\mathbf{J}^{\rm Ih}$ requires knowledge of the ionospheric electric field.

[29] Given $\mathbf{J}^{\rm Ip}$, we obtain $\mathbf{E}^{\rm I}$ from

$$F_\theta = \frac{J^{\rm Ip}_\theta}{\Sigma_{\rm p}} \qquad \text{and} \qquad E_\phi = \frac{J^{\rm Ip}_\phi}{\Sigma_{\rm p}} , \tag{13}$$

with

$$F_\theta \equiv E_\theta - \frac{2\Omega R\sin\theta}{c} B_P . \tag{14}$$

[30] This procedure does a good job of evaluating $\mathbf{E}^{\rm I}$ in the portion of the ionosphere that is magnetically connected to the outgoing tongue of magnetospheric plasma. However, it does not permit a determination of the fields that fringe this region. These control the inward flow of depleted plasma tubes.

2.8. E × B Drift

[31] Just above the ionosphere, the plasma drifts at velocity

$$\mathbf{v} = c\left(\frac{E_\phi}{2B_P}\hat{\mathbf{e}}_\theta - \frac{E_\theta}{2B_P}\hat{\mathbf{e}}_\phi\right) . \tag{15}$$

Projecting down to the magnetosphere, we obtain

$$\frac{\dot a}{a} = -\frac{2\dot\theta_0}{\theta_0} = -\frac{cE_\phi}{RB_P}\left(\frac{a}{R}\right)^{1/2} = \frac{c^2\sigma\Omega^2}{\Sigma_{\rm p}B_P^2}\left(\frac{a}{R}\right)^6 . \tag{16}$$

and

$$\frac{\Delta\Omega}{\Omega} = \frac{cF_\theta}{2\Omega RB_P}\left(\frac{a}{R}\right)^{1/2} = \frac{c^2\sigma}{2\Sigma_{\rm p}B_P^2}\left(\frac{a}{R}\right)^6\frac{\dot a}{a} . \tag{17}$$

Here $\Delta\Omega$ is the angular velocity at which the plasma in the tongue slips relative to the neutral atmosphere which at this point is assumed to be uniformly rotating. In section 4.2.1, we consider differential rotation of the ionosphere relative to the deep atmosphere.

[32] For future reference, we note that

$$\left(\frac{\dot a}{a}\right)^2 = 2\Omega\Delta\Omega . \tag{18}$$

[33] We emphasize that our expressions for $\dot a$ and $\Delta\Omega$ are valid where the plasma in the tongue is in near corotation; that is where $\dot a / (\Omega a) \ll 1$ and $\Delta\Omega / \Omega \ll 1$.

2.9. Coupling to Rate of Mass Loss

[34] Suppose the tongue covers $\Delta\phi(a)$ in azimuth, where $\Delta\phi$ is a function of a to be determined later. Then

$$\dot M = \Delta\phi a\dot a\sigma . \tag{19}$$

Substituting for $\dot a$ using equation (16), we arrive at

$$\dot M = \frac{\Delta\phi c^2\sigma^2\Omega^2R^2}{\Sigma_{\rm p}B_P^2}\left(\frac{a}{R}\right)^8 , \tag{20}$$

from which we obtain

$$\sigma = \frac{|B_P|}{c\Omega R}\left(\frac{\Sigma_{\rm p}\dot M}{\Delta\phi}\right)^{1/2}\left(\frac{R}{a}\right)^4 . \tag{21}$$

[35] Next, we replace σ in $\dot a / a$ which yields

$$\frac{\dot a}{a} = \frac{\Omega c}{R|B_P|}\left(\frac{\dot M}{\Sigma_{\rm p}\Delta\phi}\right)^{1/2}\left(\frac{a}{R}\right)^2 . \tag{22}$$

2.10. Steady State Scalings

[36] Flux freezing implies that σ / B_z is independent of a in a sourceless, steady state flow. Consequently, $\Delta\phi$ at a is related to its initial value at a_i by

$$\Delta\phi = \left(\frac{a_i}{a}\right)^2\Delta\phi_i . \tag{23}$$

Thus

$$\sigma = \frac{|B_P|}{c\Omega a_i}\left(\frac{\Sigma_{\rm p}\dot M}{\Delta\phi_i}\right)^{1/2}\left(\frac{R}{a}\right)^3 \sim 5\times10^{-12}\left(\frac{4R}{a}\right)^3 \cdot \left(\frac{\Sigma_{\rm p,13}\dot M_4}{\Delta\phi_{i,\pi}a^2_{i,4R}}\right)^{1/2} {\rm g\ cm^{-2}} . \tag{24}$$

$$\frac{\dot a}{a} = \frac{\Omega c}{a_i|B_p|}\left(\frac{\dot M}{\Sigma_{\rm p}\Delta\phi_i}\right)^{1/2}\left(\frac{a}{R}\right)^3 \sim 0.1\left(\frac{a}{4R}\right)^3 \cdot \left(\frac{\dot M_4}{\Sigma_{\rm p,13}\Delta\phi_{i,\pi}a^2_{i,4R}}\right)^{1/2} d^{-1} . \tag{25}$$

An equivalent equation was originally derived in the work of *Hill et al.* [1981].

[37] The timescale $a / \dot{a}$ for outward plasma transport decreases with distance from the planet. Plasma near the source at $a_i = 4R$ doubles its radial distance on a timescale of several days. The constancy of the observed magnetic period on far longer timescales implies that the convection pattern remains steady for many dynamical timescales of the source region.

[38] Somewhat arbitrarily, we adopt a_o, the value of a at which $\dot{a} = \Omega\, a$, or equivalently where $\Delta\Omega = \Omega / 2$, as the outer radius of the region in which partial corotation applies;

$$\left(\frac{a_o}{R}\right) = \left(\frac{a_i |B_P|}{c}\right)^{1/3} \left(\frac{\Sigma_p \Delta\phi_i}{\dot{M}}\right)^{1/6} \sim 21 \left(\frac{a_{i,4R}^2 \Delta\phi_{i,\pi} \Sigma_{p,13}}{\dot{M}_4}\right)^{1/6}. \tag{26}$$

2.11. Comparison With Previous Work

[39] We assume a steady state outflow with flux freezing and obtain $\Delta\phi \propto a^{-2}$, $\sigma \propto a^{-3}$, $\dot{a} \propto a^4$, $\Delta\Omega \propto a^6$. It is of interest to compare our results with those in the literature.

[40] *Hill* [1979] assumes steady state, axially symmetric ($\Delta\phi = 2\pi$) outward diffusive plasma transport. He derives an inertial limit on corotation, L_0, defined as the L shell at which the corotation lag, $\Delta\Omega / \Omega$, becomes of order unity. To make contact with L_0, we proceed from J_a^M [equation (6)] through J_θ^{Ip} [equation (11)] to $\Delta\Omega / \Omega$ [equation (17)]. Then we use the constancy of $\dot{M}$ [equation (19)] to eliminate $\sigma\dot{a}$ from the latter equation and set $\Delta\phi = 2\pi$. Solving for the a / R at which $\Delta\Omega / \Omega = 1/4$ yields

$$L_0 = \left(\frac{\pi \Sigma_p B_P^2 R^2}{c^2 \dot{M}}\right)^{1/4}. \tag{27}$$

[41] Hill's L_0 is related to our a_o / R in the dual limit $a_i = R$ and $\Delta\phi_i = \pi$ by $L_0 \sim (a_o / R)^{3/2}$. Corotation lags are larger in our model than in Hill's as a consequence of the decrease of $\Delta\phi$ with a. Note that the assumption of axial symmetry implies that Hill's J_ϕ^M is independent of ϕ and thus that his $J_\phi^{Ip} = 0$.

[42] The work of *Hill et al.* [1981] is the landmark paper in rotationally driven convection. It displays the complete set of governing equations and describes many salient properties of their solutions. In particular, it demonstrates that flux freezing and centrifugal balance imply $\dot{a} \propto a^4$ and deduces that a steady state plasma outflow narrows with increasing distance from its source.

[43] *Summers and Siscoe* [1982] address the same problem we do but assume $\Delta\phi$ = constant $< 2\pi$. Combining this with flux freezing ($\sigma \propto a^{-3}$), they obtain $\dot{a} \propto a^2$, $\Delta\Omega \propto a^4$. Their solution is incomplete because they do not use the relation between J_ϕ^M and J_ϕ^{Ip} [our equation (10)]; since the outflow spans $\Delta\phi < 2\pi$, the azimuthal current in the magnetosphere must close in the ionosphere via field-aligned currents at the boundaries of the tongue. The inclusion of this relation leads to our equation (16) and ultimately to the requirement that $\Delta\phi$ cannot be a constant but instead must satisfy $\Delta\phi \propto a^{-2}$.

[44] In their study of the motion of a small, isolated flux tube moving in a background of less dense plasma, *Pontius et al.* [1986] arrive at the same expressions, $\dot{a} \propto a^4$ and $\Delta\Omega \propto a^6$, as we do. As they carry out a more rigorous solution of Poisson's equation in the ionosphere, their results add weight to ours.

[45] *Hill et al.* [1981] recognized that a steady state plasma outflow must narrow with increasing distance from its source. Our specific result $\Delta\phi \propto a^{-2}$ appears to be new. Because its derivation involves approximations, it is worth reexamining from another perspective. The steady state assumption implies $\nabla \times \mathbf{E} = -\nabla \times (\mathbf{v} \times \mathbf{B}) = 0$. In cylindrical coordinates (ϖ, ϕ, z), the z component of this relation evaluated in the equatorial plane yields

$$\frac{\partial v_\phi}{\partial \phi} = 2 v_\varpi - \varpi \frac{\partial v_\varpi}{\partial \varpi}. \tag{28}$$

[46] Thus v_ϕ varies with ϕ unless $v_\varpi \propto \varpi^2$. In particular, for $v_\varpi \propto \varpi^4$,

$$\frac{\partial v_\phi}{\partial \phi} = -2 v_\varpi \tag{29}$$

from which our result $\Delta\phi \propto a^{-2}$ follows directly.

3. Magnetic Perturbations

3.1. Observations and Assumptions

[47] *Giampieri et al.* [2006] found all three spatial components of the nonaxisymmetric magnetic field to be of the same magnitude (several nanotesla), to exhibit the same periodicity, and to display a weak dependence on distance from the planet. The ϕ component was measured with the highest signal-to-noise ratio.

[48] Figure 1 displays the currents associated with the plasma tongue. The magnetic perturbations created by these currents are discussed in what follows. We calculate these under the assumption of $\Delta\,\Omega \ll \Omega$, i.e., a straight tongue. Ionospheric conductivities are expected to be larger in the summer hemisphere, so we neglect those currents presently flowing north of the equator. Expected departures from this simple picture will be discussed in section 3.4. Because *Giampieri et al.* [2006] highlighted the azimuthal magnetic perturbations, we make particular effort to calculate these. We focus on perturbations in the inner magnetosphere ($a \sim 4{-}8\ R_S$) where the measurements were made.

3.2. Magnetic Perturbations From Currents in the Tongue

[49] Directly above and below the tongue, J_ϕ^M gives rise to a radial magnetic perturbation, B_a, of magnitude

$$|B_a| = \frac{2\pi J_\phi^M}{c} \sim 6 \times 10^{-6} \left(\frac{a}{a_i}\right) \left(\frac{\dot{M}_4 \Sigma_{p,13}}{\Delta\phi_{i,\pi}}\right)^{1/2} \mathrm{G}, \tag{30}$$

where the final relation is obtained using equations (5) and (24). The radial current in the tongue, J_a^M, is much smaller than J_ϕ^M in the inner magnetosphere,

$$\frac{J_a^M}{J_\phi^M} \sim 0.01 \left(\frac{a}{a_i}\right)^3 \left(\frac{\dot{M}_4 a_{i,4R}^6}{\Delta\phi_{i,\pi} \Sigma_{p,13}}\right)^{1/2}. \tag{31}$$

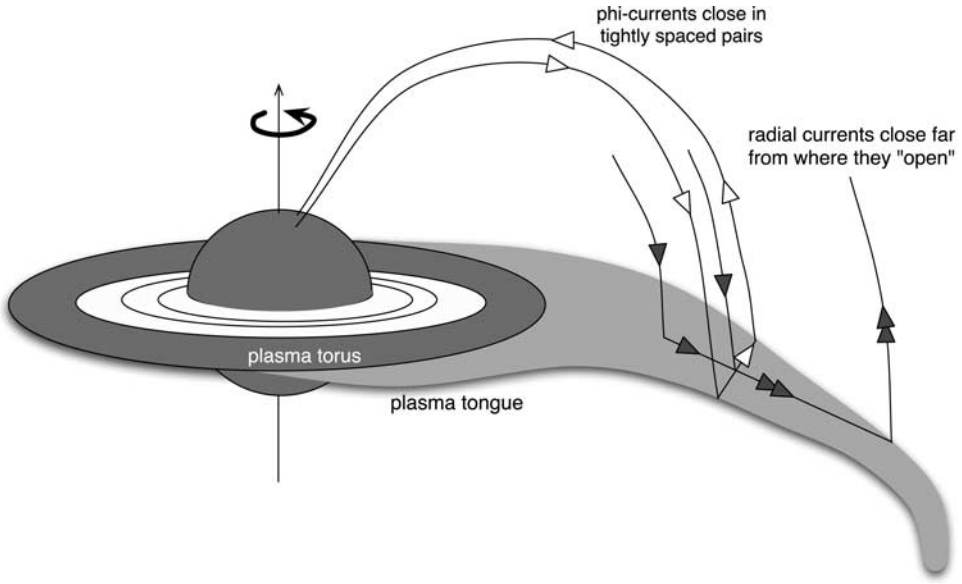

Figure 1. The currents associated with the plasma tongue in Saturn's magnetosphere.

Consequently, the azimuthal magnetic perturbation it produces is much smaller than that reported by *Giampieri et al* [2006], and we neglect it.

3.3. Dominant Contribution to B_ϕ

[50] From equations (23), (31), and (30), we see that the total radial current in the tongue at a,

$$I \sim J_a^{\mathrm{M}} a \Delta\phi \sim \frac{2c\Omega\dot{M}}{B_p}\left(\frac{a}{R}\right)^3, \tag{32}$$

increases sharply with distance from Saturn. As a result, the dominant azimuthal magnetic perturbations in the inner magnetosphere are produced by the current that flows along magnetic field lines which connect the summer polar ionosphere to the outer part of the tongue near a_{o}. Field lines crossing the equator near $a \sim a_{\mathrm{o}}$ carry a current of order I_{o}, where

$$I_{\mathrm{o}} \sim \frac{2c\Omega\dot{M}}{B_p}\left(\frac{a_o}{R}\right)^3 \sim 2\Omega a_i\left(\Delta\phi_i \dot{M}\Sigma_{\mathrm{p}}\right)^{1/2}. \tag{33}$$

We approximate the resulting magnetic perturbations as arising from a "wire" of field-aligned current I_{o} arching over the inner magnetosphere. The smallest distance s between an observer in the equator plane at a and a field line that passes through the equator at a much larger distance a_0 is $s \sim a$. We thus estimate the magnetic perturbation from the field-aligned currents to be

$$B_\phi \sim -\frac{2I_{\mathrm{o}}}{cs} \sim -1.2\times 10^{-5}\left(\frac{a_i}{a}\right)\left(\Delta\phi_{i,\pi}\dot{M}_4\Sigma_{\mathrm{p},13}\right)^{1/2}\mathrm{G}. \tag{34}$$

3.4. Commentary and Caveats

[51] The above calculations yield values of B_a and B_ϕ of the same order as those found by *Giampieri et al.* [2006], with weak radial variations, $B_a \propto a$; $B_\phi \propto a^{-1}$. At longitudes not coincident with the plasma tongue, these perturbations will mix into approximately equal parts of the three spatial magnetic field components a, θ, ϕ.

[52] The above estimate for the magnitude of B_ϕ ignores the contribution from the return current that comes from $a > a_{\mathrm{o}}$ and closes the circuit. Unfortunately, not much can be deduced about the geometry of the return current since the field lines it flows along are likely to be strongly perturbed by the solar wind. However, it is possible that it could act to reduce the magnitude of the perturbation by a factor 2 or more. Conversely, fragmentation of the tongue into narrower structures would not greatly affect the estimated B_ϕ, since magnetic perturbations from individual fingers would add coherently.

[53] We have also ignored the contribution from the currents that flow in the northern hemisphere. In the case of perfect N-S symmetry, magnetic perturbations from the two hemispheres would exactly cancel B_ϕ in the middle of the tongue but not elsewhere. In reality, at most times (the exception being near times of equinox), this cancellation is likely to be small, since the ionospheric conductivity will differ significantly in the northern and southern polar ionospheres. Near solstice, almost all the current will flow through the summer hemisphere. At these times, the above estimate for B_ϕ should be approximately doubled.

[54] Importantly, the approximation $\Delta\Omega \ll \Omega$ is not valid in the outer part of the tongue, and we expect significant curvature as corotation lags become large. Under the assumption of a straight tongue, the perturbations $|B_a|$ and $|B_\phi|$ are in phase with each other and also in phase with the maximum plasma density (south of the equator, B_a and B_ϕ are in phase; to the north, they have opposite phase). In reality, we expect $|B_\phi|$ to significantly lag the maximum plasma density in the inner magnetosphere, since B_ϕ originates from currents feeding the end of the tongue.

[55] The largest field-aligned currents occur close to a_{o}, where the tongue spans a narrow range of longitudes. We propose that the SKR is associated with these currents,

and as such displays the same periodicity as the magnetic field.

4. The Clock

[56] As described in section 1, a somewhat slow and imperfect clock controls the quasiperiodic behavior of SKR bursts. In our scenario, the same clock controls the nonaxisymmetric magnetic perturbations. Both Voyager- and Cassini-era measurements of SKR and magnetic periods are consistent with this picture.

4.1. Where is the Clock Located?

[57] We hypothesize that the clock beats at the period of rotation of the asymmetry associated with the inner portion of the plasma outflow. Ionization of water vapor ejected from Enceladus at $a \approx 4R$ is the dominant plasma source. As explained below, the clock's period propagates throughout the magnetosphere provided the differential rotation of the latter remains time invariant.

[58] Suppose that a source of material located at radius a_i feeds a plasma torus rotating at Ω_i. The torus is unstable and sends out a "tongue" of plasma centered on a fixed azimuth $\phi_c(a_i)$ in the rotating frame. Plasma at the center of the tongue moves outwards at radial speed $\dot{a}_c(a)$ and rotates at angular speed $\dot{\phi}_c(a)$, where $\dot{\phi}_c(a) \lesssim \Omega_i$. In steady state, the shape of the tongue's centerline would be determined by

$$\phi_c(a) = \phi_c(a_i) + \int_{a_i}^{a} \mathrm{d}a' \, \frac{\dot{\phi}_c(a')}{\dot{a}_c(a')} \,. \tag{35}$$

[59] Viewed from a nonrotating frame, the tongue is a steady structure rotating at pattern speed Ω_i. At radius a and time t, the apparent azimuth of the tongue's centerline is given by

$$\phi_{\rm obs} = \phi_c(a) + \Omega_i t, \tag{36}$$

and so $\dot{\phi}_{\rm obs} = \Omega_i$, regardless of the run of differential rotation across the magnetosphere.

4.2. Why is the Clock Slow?

[60] SKR and magnetic periods determined by Cassini are longer than those associated with the motion of any atmospheric features. The most plausible explanation is that the ionosphere rotates more slowly than the underlying atmosphere because magnetic torques are transferring angular momentum from it to the plasma tongue. *Huang and Hill* [1989] conclude that the rotation of Jupiter's ionosphere is slowed in this manner.

[61] Since the magnetic torque increases sharply with increasing latitude, this is also a plausible explanation for the observed decline of the magnetosphere's angular velocity with increasing distance from Saturn. This scenario is quantitatively reasonable, in contrast to models based on the slippage of the rotation of the magnetospheric plasma relative to the rotation of the ionosphere. The observed clock frequency is the rotation rate of the ionosphere where it connects to the inner part of the plasma tongue.

4.3. Steady State Rotation of the Ionosphere

[62] We analyze a simple model for the steady state rotation of the ionosphere and underlying atmosphere. It assumes axial symmetry and considers only vertical transport of angular momentum. Deep atmospheric layers are taken to rotate rigidly with angular velocity Ω. We work within the approximation of an isothermal atmosphere with sound speed c_s, scale height $H = c_s^2 / \gamma g$, buoyancy frequency $N^2 = (\gamma-1)g / (\gamma H)$, and eddy diffusivity ν. The ionosphere is taken to be a single layer rotating at the angular velocity $\Omega^{\rm M}$ of the part of the plasma tongue to which it is magnetically connected.

[63] We modify equation (6) to allow for the nonuniform rotation rate, $\Omega^{\rm M}$, of the magnetospheric plasma. The torque per unit a applied to the tongue of outgoing plasma reads

$$\frac{\mathrm{d}T_B^{\rm M}}{\mathrm{d}a} = \dot{M} \frac{\mathrm{d}}{\mathrm{d}a} \left(\Omega^{\rm M} a^2\right) . \tag{37}$$

Thus the magnetic torque per unit θ_0 on the ionosphere is given by

$$\frac{\mathrm{d}T_B^{\rm I}}{\mathrm{d}\theta_0} = \frac{\dot{M}R^2}{2} \frac{\mathrm{d}}{\mathrm{d}\theta_0} \left(\frac{\Omega^{\rm M}}{\theta_0^4}\right) . \tag{38}$$

In steady state, the torque must be constant with depth below the ionosphere. Provided the torque is not too large, a stable, steady state, shear flow is established in which the viscous torque given by

$$\frac{\mathrm{d}T_\nu}{\mathrm{d}\theta_0} = -2\pi R^4 \theta_0^3 \rho \nu \frac{\mathrm{d}\Omega^A}{\mathrm{d}z} \,, \tag{39}$$

carries angular momentum up from the atmosphere to the ionosphere. Equating the viscous torque to the magnetic torque yields

$$\frac{\mathrm{d}\Omega^A}{\mathrm{d}z} = \frac{\dot{M}}{4\pi R^2 \rho \nu \theta_0^3} \frac{\mathrm{d}}{\mathrm{d}\theta_0} \left(\frac{\Omega^{\rm M}}{\theta_0^4}\right) . \tag{40}$$

The shear flow is stable where the Richardson criterion is satisfied, that is where equation (40) predicts

$$R\theta_0 \frac{\mathrm{d}\Omega^A}{\mathrm{d}z} \lesssim N \,. \tag{41}$$

In the stable regime,

$$\Omega - \Omega^{\rm M} \approx -\frac{\dot{M}H}{4\pi R^2 \rho^I \nu \theta_0^3} \frac{\mathrm{d}}{\mathrm{d}\theta_0} \left(\frac{\Omega^{\rm M}}{\theta_0^4}\right) \approx \frac{\dot{M}\Omega H a^4}{\pi R^2 \rho^{\rm I} \nu R^4} \,. \tag{42}$$

Here we have set $\Omega^{\rm M} = \Omega$ in the final step. This is a good approximation since $\Omega - \Omega^{\rm M} \ll \Omega$ in the stable regime.

[64] The boundary of the stable regime occurs where the stability criterion is violated just below the ionosphere. We use the symbol Θ_0 to denote the value of θ_0 at this boundary. At Θ_0,

$$\frac{\dot{M}}{4\pi R \rho^{\rm I} \nu N \Theta_0^2} \frac{\mathrm{d}}{\mathrm{d}\theta_0} \left(\frac{\Omega^{\rm M}}{\theta_0^4}\right) \approx -1 \,. \tag{43}$$

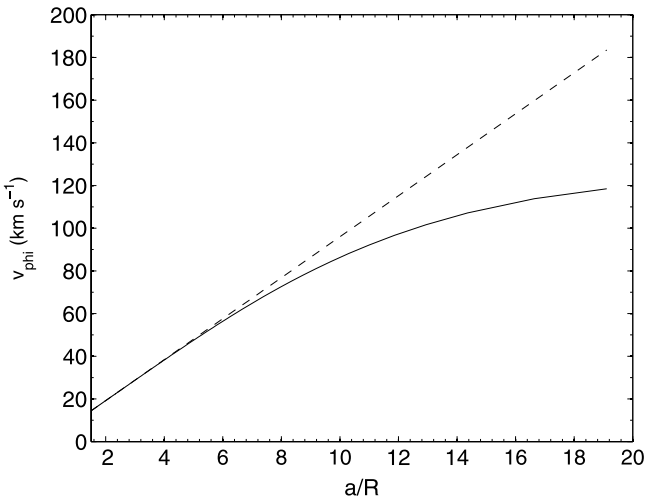

Figure 2. Rotational velocity of equatorial plasma as a function of distance from Saturn. Rigid corotation with Saturn's interior is plotted as the dashed line; the magnetosphere lags the planetary interior due to slowing of the ionosphere by magnetic torques.

An approximate solution for Θ_0, and the corresponding $a_{\rm crit}/R \equiv \Theta_0^{-2}$, follows from setting $\Omega^{\rm M} = \Omega$. In this manner, we arrive at

$$\frac{a_{\rm crit}}{R} = \left(\frac{1}{\Theta_0^2}\right) \approx \left(\frac{\pi R \rho^{\rm I} \nu N}{\dot{M}\Omega}\right)^{2/7} \sim 9.1 \left(\frac{\nu_8 \rho^I_{-12.5}}{\dot{M}_4 T_{140}^{1/2}}\right)^{2/7}. \quad (44)$$

[65] Turbulent diffusion enhances the rate at which angular momentum is transported upward in regions where the atmosphere is Richardson unstable. This slows the rate at which the corotation lag increases with increasing $a > a_{\rm crit}$ [*Pontius*, 1997]. To assess this rate, we determine the depth to which the unstable layer penetrates into the atmosphere. Because the angular velocity gradient in a stable layer is inversely proportional to density, and the density increases exponentially with depth, the thickness of the unstable layer increases logarithmically with decreasing θ_0. An estimate for $\Omega - \Omega^{\rm M}$ is obtained by multiplying the critical angular velocity gradient from equation (41) by the thickness of the unstable layer. The following expression provides a good fit to $\Omega - \Omega^{\rm M}$ for all values of θ_0 or a/R. We express it in terms of the latter for ease of comparison with data on the rotation of plasma in Saturn's magnetosphere.

$$1 - \frac{\Omega^{\rm M}}{\Omega} \approx \frac{NH}{\Omega R}\left(\frac{a}{R}\right)^{1/2} \ln\left[1 + \left(\frac{a}{a_{\rm crit}}\right)^{7/2}\left(\frac{\Omega^{\rm M}}{\Omega} + \frac{a}{2\Omega}\frac{{\rm d}\Omega^{\rm M}}{{\rm d}a}\right)\right]. \quad (45)$$

[66] Figure 2 displays the run of $v_\phi = \Omega^{\rm M} a$ versus a/R for our nominal parameters. The rotation curve is in reasonable agreement with Voyager measurements [*Richardson*, 1986]. At $a/R = 4$, corresponding to the orbit of Enceladus, $1 - \Omega^{\rm M}/\Omega \simeq 0.5\%$. By comparison, equation (18) predicts the much smaller value, 3×10^{-5}, for the slippage of the rotation rate in the plasma tongue at $a = 4R$ relative to that of the ionosphere.

4.4. Why is the Clock so Steady?

[67] We have tentatively associated the clock's period with that of the rotation of plasma in the vicinity of the orbit of Enceladus. This period, which reflects the lag of the ionosphere's rotation relative to that of the underlying atmosphere, depends upon only two parameters, ν and $\dot{M}$ (see equation 45). Unfortunately, little is known about the temporal variations of either.

[68] The clock rate has varied by $\approx$1% around a mean value that is of order 1% slower than the rotation period of clouds in Saturn's equatorial jet. This implies a small corotation lag, and a consequently shear stability, of the ionosphere that is coupled to the plasma near Enceladus. It also implies that our choice of eddy viscosity, $\nu \approx 10^8$ cm^2 s^{-1}, is not far off the mark. The ionosphere would respond to changes in $\dot{M}$ on the diffusion time

$$\tau_\nu \sim \frac{H^2}{\nu} \sim 10^5 \, {\rm s}, \quad (46)$$

which is much shorter than the timescale for observed changes in the clock rate. The timescale for outflowing plasma near the orbit of Enceladus to double its distance from Saturn is also short, of order several days (see equation 25).

[69] The stability of the clock on a yearlong timescale poses a problem since the rate at which Enceladus ejects mass seems to vary on a much shorter timescale [*Jones et al.*, 2006]. A possible solution involves the slow rate at which neutral molecules are ionized (cf. the discussion in section 2.1). This acts to smooth variations in their number density that result from variations in the rate of mass ejection from Enceladus.

5. Summary

[70] Rotationally driven convection of magnetospheric plasma breaks the axisymmetry of the external magnetic field at Saturn. Field-aligned currents transfer angular momentum from the planet to a tongue of outflowing

plasma. This transfer slows the rate of rotation of the ionosphere relative to that of the underlying atmosphere. The currents are the source for the nonaxisymmetric components of the magnetic field. The common rotation rates of these components and SKR bursts is that of the plasma near the orbit of Enceladus and by extension the rotation rate in the ionosphere to which this plasma is coupled. This tells us nothing about the rotation rate of Saturn's deep interior. Of that we remain ignorant.

[71] Magnetic perturbations with magnitudes similar to those observed by Cassini are produced for $\dot{M} \sim 10^4$ g s^{-1}, a value similar to estimates for the rate of production of plasma from water vapor ejected from Enceladus.

[72] Enhancement of the SKR occurs in a narrow range of longitudes where large currents flow along magnetic field lines connecting the tip of the plasma stream to the auroral ionosphere.

[73] **Acknowledgments.** Wolfgang Baumjohann thanks the reviewers for their assistance in evaluating this paper.

References

Atreya, S. K., T. M. Donahue, A. F. Nagy, J. H. Waite Jr., and J. C. McConnell (1984), Theory, measurements, and models of the upper atmosphere and ionosphere of Saturn, in *Saturn* (A85-33976 15-91), edited by T. Gehrels and M. S. Matthews, pp. 239–277, Univ. of Arizona Press, Tucson.

Chen, C.-K. (1977), Topics in planetary plasmaspheres. Ph.D. thesis, UCLA, Los Angeles, California.

Desch, M. D., and M. L. Kaiser (1981), Voyager measurement of the rotation period of Saturn's magnetic field, *Geophys. Res. Lett.*, *8*, 253–256.

Dessler, A. J., and T. W. Hill (1975), High-order magnetic multipoles as a source of gross asymmetry in the distant Jovian magnetosphere, *Geophys. Res. Lett.*, *2*, 567–570.

Dessler, A. J., and T. W. Hill (1979), Jovian longitudinal control of Io-related radio emissions, *Astrophys. J.*, *227*, 664–675.

Galopeau, P. H. M., and A. Lecacheux (2000), Variations of Saturn's radio rotation period measured at kilometer wavelengths, *J. Geophys. Res.*, *105*, 13,089–13,102.

Giampieri, G., and M. K. Dougherty (2004), Rotation rate of Saturn's interior from magnetic field observations, *Geophys. Res. Lett.*, *31*, 16,701, L16701, doi:10.1029/2004GL020194.

Giampieri, G., M. K. Dougherty, E. J. Smith, and C. T. Russell (2006), A regular period for Saturn's magnetic field that may track its internal rotation, *Nature*, *441*, 62–64.

Gurnett, D. A., et al. (2005), Radio and Plasma wave observations at Saturn from Cassini's approach and first orbit, *Science*, *307*, 1255–1259.

Gurnett, D. A., A. M. Persoon, W. S. Kurth, M. K. Dougherty, and D. J. Southwood (2006), The rotational modulation of the electron density in Saturn's plasma disk, *AGU*, Fall Meeting Abstracts 4.

Hansen, C. J., L. Esposito, A. I. F. Stewart, J. Colwell, A. Hendrix, W. Pryor, D. Shemansky, and R. West (2006), Enceladus' water vapor plume, *Science*, *311*, 1422–1425.

Hill, T. W. (1979), Inertial limit on corotation, *J. Geophys. Res.*, *84*, 6554–6558.

Hill, T. W., A. J. Dessler, and L. J. Maher (1981), Corotating magnetospheric convection, *J. Geophys. Res.*, *86*, 9020–9028.

Huang, T. S., and T. W. Hill (1989), Corotation lag of the Jovian atmosphere, ionosphere, and magnetosphere, *J. Geophys. Res.*, *94*, 3761–3765.

Johnson, R. E., H. T. Smith, O. J. Tucker, M. Liu, M. H. Burger, E. C. Sittler, and R. L. Tokar (2006), The Enceladus and OH Tori at Saturn, *Astrophys. J.*, *644*, L137–L139.

Jones, G. H., E. Roussos, N. Krupp, C. Paranicas, J. Woch, A. Lagg, D. G. Mitchell, S. M. Krimigis, and M. K. Dougherty (2006), Enceladus' varying imprint on the magnetosphere of Saturn, *Science*, *311*, 1412–1415.

Jurac, S., M. A. McGrath, R. E. Johnson, J. D. Richardson, V. M. Vasyliunas, and A. Eviatar (2002), Saturn: Search for a missing water source, *Geophys. Res. Lett.*, *29*(24), 2172, doi:10.1029/2002GL015855.

Krupp, N., et al. (2004), Dynamics of the Jovian magnetosphere, in *Jupiter. The Planet, Satellites and Magnetosphere*, pp. 617–638, edited by Fran Bagenal, Timothy E. Dowling, and William B. McKinnon, ISBN 0-521-81808-7, Cambridge University Press, Cambridge, UK.

Leisner, J. S., C. T. Russell, M. K. Dougherty, X. Blanco-Cano, R. J. Strangeway, and C. Bertucci (2006), Ion cyclotron waves in Saturn's E ring: Initial Cassini observations, *Geophys. Res. Lett.*, *33*, L11101, doi:10.1029/2005GL024875.

Pontius, D. H., Jr., T. W. Hill, and M. E. Rassbach (1986), Steady state plasma transport in a corotation-dominated magnetosphere, *Geophys. Res. Lett.*, *13*, 1097–1100.

Pontius, D. H., Jr. (1997), Radial mass transport and rotational dynamics, *J. Geophys. Res.*, *102*, 7137–7150.

Pontius, D. H., Jr., and T. W. Hill (1989), Rotation driven plasma transport—The coupling of macroscopic motion and microdiffusion, *J. Geophys. Res.*, *94*, 15,041–15,053.

Pontius, D. H., Jr., and T. W. Hill (2006), Enceladus: A significant plasma source for Saturn's magnetosphere, *J. Geophys. Res.*, *111*, A09214, doi:10.1029/2006JA011674.

Richardson, J. D. (1986), Thermal ions at Saturn—Plasma parameters and implications, *J. Geophys. Res.*, *91*, 1381–1389.

Shemansky, D. E., P. Matheson, D. T. Hall, H.-Y. Hu, and T. M. Tripp (1993), Detection of the hydroxyl radical in the Saturn magnetosphere, *Nature*, *363*, 329–331.

Summers, D., and G. L. Siscoe (1982), Solutions to the equations for corotating magnetospheric convection, *Astrophys. J.*, *261*, 677–683.

Tokar, R. L., et al. (2006), The interaction of the atmosphere of Enceladus with Saturn's plasma, *Science*, *311*, 1409–1412.

Wu, H., T. W. Hill, R. A. Wolf, and R. W. Spiro (2007), Numerical simulation of fine structure in the Io plasma torus produced by the centrifugal interchange instability, *J. Geophys. Res.*, *112*, A02206, doi:10.1029/2006JA012032.

Yang, Y. S., R. A. Wolf, R. W. Spiro, T. W. Hill, and A. J. Dessler (1994), Numerical simulation of torus-driven plasma transport in the Jovian magnetosphere, *Journal of Geophysical Research*, *99*, 8755–8770.

A. J. Farmer, Department of Astronomy, Harvard University, MS-51, 60 Garden St, Cambridge, MA 02138, USA. (afarmer@cfa.harvard.edu)

P. Goldreich, Institute for Advanced Study, Princeton, NJ 08540, USA. (pmg@ias.edu)